Ocean Wave Prediction by a Hybrid Model - Combination of Single-Parameterized Wind Waves with Spectrally Treated Swells

Sci. Rep. Tôhoku Univ., Ser. 5, (Tôhoku Geophys. Journ.), Vol. 28, No. 1, pp. 27–45, 1981.

Ocean Wave Prediction by a Hybrid Model — Combination of Single-Parameterized Wind Waves with Spectrally Treated Swells

PAIMPILLIL S. JOSEPH**, SANSHIRO KAWAI
and YOSHIAKI TOBA

Geophysical Institute, Faculty of Science, Tohoku University
Sendai 980, Japan

(Received March, 16, 1981)

Abstract: The single parameter wind wave growth equation proposed by Toba and the grid interpolation method used in the authors' previous paper are combined with a spectral treatment for the swells, to produce an ocean wave prediction model. The predicted waves in the intense winds associated with low pressure systems clearly demonstrate the model's ability in reproducing the spatial and temporal trends in the wave development. The present spectral treatment of swells, performed by introducing interchange between swells and wind waves having the self-similar simple spectral form, is found to be sufficient in providing good spectral representation of the wave field.

1. Introduction

It has been recognized by many investigators that there is a similarity structure in the growing wind wave field. Due to this similarity, the complexity in the practical wave predictions is reduced considerably though the theoretical works on wave growth are not reached up to the stage of its direct usage in the ocean wave predictions. Using the similarity concepts, Toba (1972) proposed a power law type relation between the significant wave height and significant wave period. Toba (1973) also proposed a simple spectral form for the wind waves for the high frequency side. Mitsuyasu *et al.* (1980) had shown that there is quasi-equivalence between Toba's spectrum and JONSWAP-type spectrum of Hasselmann *et al.* (1973) in the high frequency side. With the usage of the similarity based power law and the spectral form, Toba (1978) proposed a single parameter growth equation for the wind wave part of the ocean waves. This single parameter equation forms the basis of the prediction of the wind wave part in the present model.

The above single parameter growth equation was already used in wave hindcasting by Kawai *et al.* (1979) and Joseph *et al.* (1981), and its applicability was substantiated. The relative merits of using this growth equation were well described in the above two papers. In both of them, swell field was treated by some empirical relationships given

** On leave of absence from Physical Oceanography Division, National Institute of Oceanography, N.I.O. Post, Donapaula, 403004, INDIA

by Bretschneider (1968), which gave only the gross nature of the swells. For incorporating the influences of strong and opposing winds on swells and also to get the spectral form of the swell field, spectral concepts are introduced in the present model in the treatment of swells. This is the main part which is different from the earlier prediction trials using the same single parameter equation. The spectral treatment for the swell part is somewhat similar to the swell treatment in Günther *et al.* (1979). The usage of the single parameter part for wind waves along with the spectral concepts for the swells gives the hybrid nature to the present model.

2. Numerical scheme of hybrid model with basic equations

2.1. The 3/2 power law

With dimensional and macroscopic considerations Toba (1972) proposed the 3/2 power law as:

$$H_s^* = BT_s^{*3/2} \tag{1}$$

where $H_s^* \equiv g H_s/u_*^2$, $T_s^* \equiv g T_s/u_*$ and $B=0.062$ with H_s, T_s and u_* as significant wave height, significant wave period and friction velocity of air, respectively, and g as the acceleration due to gravity. This power law relationship was later extended to the individual waves in the main part of the wind wave spectrum by Tokuda and Toba (1981). The above power law relation was also convertible (Toba, 1978) into a relation between the total energy E of the wind waves and the peak frequency f_p as:

$$E^* = B_f f_p^{*-3}, \qquad B_f = 2.1\times 10^{-4} \tag{2}$$

where $E^* \equiv g^2 E/u_*^4$, $f_p^* \equiv u_* f_p/g$ with f_p correlated with T_s by

$$f_p = (1.05\, T_s)^{-1} \tag{3}$$

according to Mitsuyasu (1968) and Toba (1973). In the course of the derivation of the energy equation, the relation

$$E = \int_0^\infty \phi(f)\, df = H_s^2/16 \tag{4}$$

after Longuet-Higgins (1952) was also utilized, where $\phi(f)$ is the frequency spectrum.

2.2. Spectral form

As to the spectral form, the present model assumes a complete self-similarity form. The frequency spectrum of the high frequency side is expressed by Toba (1973) as:

$$\phi(f) = (2\pi)^{-3}\, \alpha g_* u_*\, f^{-4}, \qquad \alpha = 0.062 \tag{5}$$

where $g_* \equiv g(1+Sk^2/\rho g)$ with S as surface tension, k wave number and ρ water density. For the low frequency side of the wind wave spectrum, a symmetrical form of the Toba spectrum on a log-log diagram as shown in Fig. 1 is assumed and then the spectral form on both sides of the spectral peak (excluding the capillary wave range) is as follows:

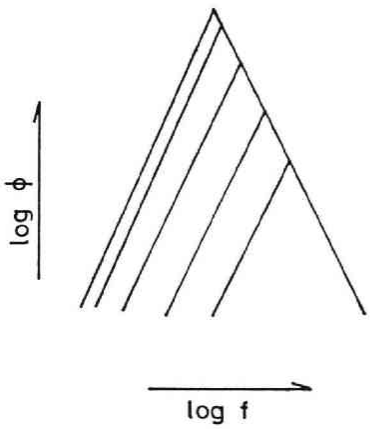

Fig. 1. Schematic representation of the present symmetrical and self-similar one-dimensional spectrum form for wind waves.

$$\phi(f) = \begin{cases} (2\pi)^{-3}\,\alpha g u_* f^{-4} & \text{for } (f \geq f_p) \\ (2\pi)^{-3}\,\alpha g u_* f_p^{-8} f^4 & \text{for } (f < f_p) \end{cases} \tag{6}$$

The value of the constant α is re-calculated in the following way. From (6), the total energy of the wind wave spectrum is

$$E = \int_0^\infty \phi(f)\, df = (2\pi)^{-3}\,(8/15)\,\alpha g u_* f_p^{-3} \tag{7}$$

and then by the usage of the equation (2), some additional calculations give

$$\alpha = 0.096 \tag{8}$$

Using field data collected from an oceanographic tower station, Kawai *et al.* (1977) has given a value of $\alpha = 0.062 \pm 0.010$. But, using the data collected from buoys, Mitsuyasu *et al.* (1980) had proposed a weak dependece of α on fetch with its values ranging from 0.06 to 0.12. The value of α obtained by the simple calculations of the present takes the mid-value of the range given by Mitsuyasu *et al.* (1980).

2.3. *Single parameter growth equation*

Using the above mentioned similarity and the empirical relationship of significant wave period with fetch given in Wilson (1965), Toba (1978) had proposed a single parameter growth equation for wind waves, of which the total derivative form is expressed as:

$$\frac{dE^{*2/3}}{dt^*} = G_0 R\,[1 - \text{erf}\,(bE^{*1/3})]\,, \tag{9}$$

where $t^* \equiv gt/u_*$, $G_0 R = 2.4 \times 10^{-4}$, $b = 0.12$ and

$$\text{erf}\,(x) \equiv 2\pi^{-1/2} \int_0^x \exp(-t^2)\, dt\,. \tag{10}$$

The nondimensional wave energy E^* attains a saturated value for a fully developed

state. The saturated energy value corresponds to the fully developed condition $c/U=1.37$ of Wilson (1965), where U is the mean wind speed at the 10 m level and c the phase velocity. With the use of a drag coefficient of 1.2×10^{-3} in the above condition, the fully developed state corresponds to a nondimensional peak period $T_s{}^*=248$ or to the nondimensional wind wave energy $E^*=3.7\times10^3$ in the present.

2.4. *Prediction scheme for the wind waves*

The present prediction equation for the wind waves is a first order differential equation which can be easily integrated numerically. A flow chart of the wind wave prediction along with the swell formation conditions is shown in Fig. 2. The conditions of zero initial energy for the entire prediction region and of no energy flow into the prediction region from outside through the numerical boundaries, as in Kawai *et al.* (1979) and in Joseph *et al.* (1981), are used in the present also. The basic equation is integrated with the iteration scheme in Kawai *et al.* (1979), and the grid interpolation method in Joseph *et al.* (1981) is also used in the present model without any modification. Though the swell formation by the wind wave saturation or by wind direction shifts remains as the same in the above two references, the treatment of the

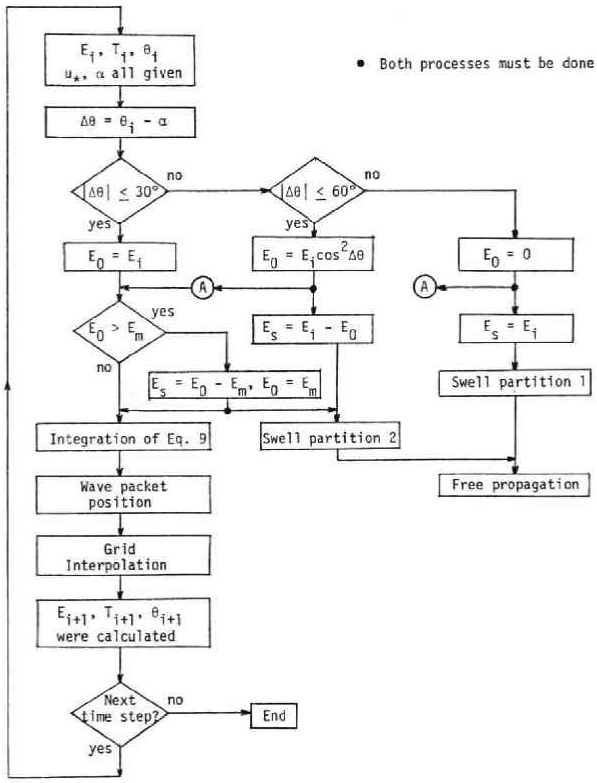

Fig. 2. Main scheme of the model. The α represents wind direction, θ the wave direction, E_s the total swell energy and E_m the saturated wind wave energy.

swell field is completely different and this will be described in detail in the next section.

2.5. *Prediction scheme for swells*

Once swell formation occurs, swells need to be propagated in prediction region with some suitable scheme. For simplicity and with economical considerations it can be done with available empirical relations which predict the gross nature of a swell field. In the empirical treatment used in Kawai *et al.* (1979) and Joseph *et al.* (1981), any treatment of a possible interchange to wind waves during its propagation through strong wind region and an energy partition of the original swell field into spectral swell components are lacking. For including these two points, spectral concepts need to be introduced to swell field at the time of its formation and in its subsequent propagation stage. This means that a swell field needs to be separated into a number of frequency components and be propagated as nearly free water waves undergoing interchange to wind waves or decay in accordance with winds prevailing in propagation region.

Swells are assumed to have one direction nature with the selected frequency components ranging from 0.04 to 0.15 Hz of 0.01 Hz frequency bands as shown in Fig. 3 with the energy density at the formation time corresponding to the one directional spectrum of wind waves. For frequencies greater than 0.15 Hz, the energy is cut off since the energy density is small. This limitation in the number of frequency bands was introduced by the limitation of the computer memory. According to the formation process of the swell, the energy partition into the above frequency bins is given in different ways. The swell partition 2 shown in Fig. 3, corresponds to swell formation

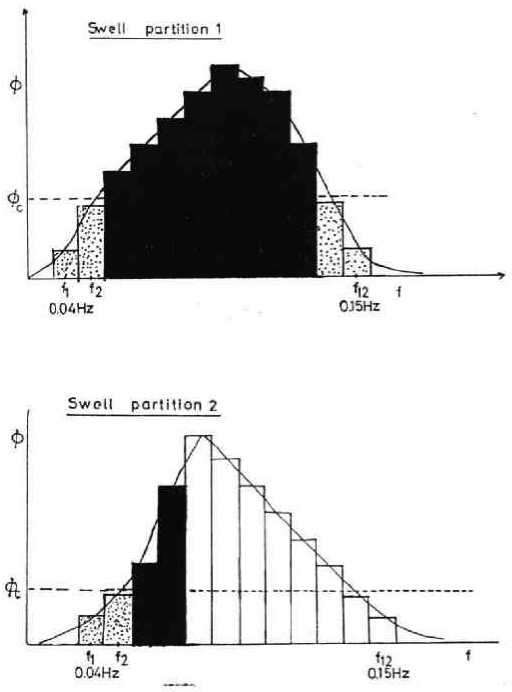

Fig. 3. Schematic illustration of swell partition. The area with dots and shade corresponds to the swell energy E_s, and that with shade only propagates as swells. The ϕ_c stands for cut off energy level.

by wind wave energy saturation or by wind direction change $|\Delta\theta| \leq 60°$ ($\Delta\theta$=wind direction−wind wave direction). The swell partition 1 shown in Fig. 3, corresponds to swell formation due to wind direction change $|\Delta\theta|$ greater than 60°. In both the partitions, ϕ_c is an energy cut off level to neglect minor swell packets. As to the value of ϕ_c, it will be reasonable to adopt a value of the peak energy level of saturated wind waves with a peak frequency at the uppermost swell band. In the swell partition 1, only the dark area is considered. In swell partition 2, dark area's energy only propagated as swells, the white area remains as the energy of the wind waves. The dotted portion's energy which remains below the cut off energy level is neglected.

The scheme for the free propagation of swell is shown as a flow chart in Fig. 4. The subscript j is the frequency number. After the phase speed c is estimated, readjustment is made by use of the wind at the nearest grid to the swell's newly attained position. Namely, for an adverse wind of $|\Delta\theta| > 90°$, swells propagate in the original direction but decaying by Inoue's (1967) formula:

$$B(f, u_*) = \{0.00139 \exp[-7000\{(u_*/c) - 0.031\}^2] + 0.725(u_*/c)^2 \exp[-0.0004(c/u_*)^2]\} f \qquad (11)$$

where f is the frequency. For $|\Delta\theta|$ between 60° and 90°, swells propagate as free waves, for $|\Delta\theta|$ smaller than 60° the energy of the components of $c/U < 1.37$ is again added to the wind wave energy, otherwise freely propagated.

At the stage of the output of swell packets, 12 directional bins of 30° are used, and for a particular bin the swell component having maximum energy in each frequency band is adopted and it is assumed to take the mid-angle of the bin.

This hybrid model now makes it possible to provide the entire spectrum of wave field at any grid point by a superposition of the combined energy of a swell component from all directions with available energy of the wind wave component of same frequency. A directional spectrum may also be possible if a directional spreading function is applied

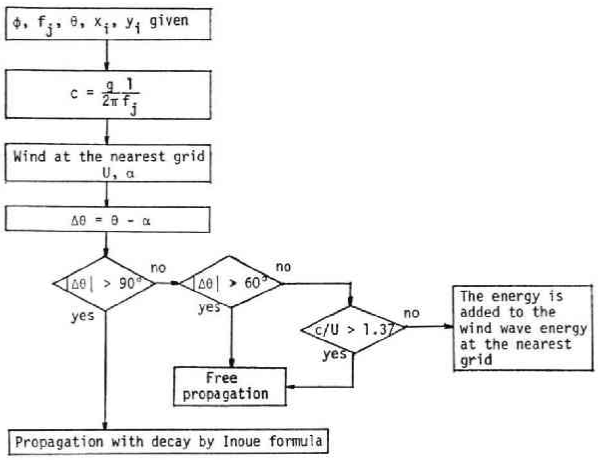

Fig. 4. Scheme for free propagation of swells. The (x_i, y_i) stands for the position of the swell component.

to the wind wave spectrum and then by the addition of the frequency-directional swell components to the wind wave directional spectrum.

3. Field test of hybrid model

The ability of the present model to represent wave development and spectral distribution of wave energy is tested for wind systems which change in intensity and direction with space and time. During the testing, two wind data corresponding to intense low pressure systems are used. In the two trials, the grid size and the time step of integration are changed according to the areal extent of the prediction region. Each of the cases is separately looked in the following.

3.1. Hindcasts in intense low pressure systems of Atlantic

In this trial, the wind and wave data of the Atlantic cyclone of December 1959, which is well described in Bretschneider *et al.* (1962) are used. In addition to the time interval considered in Kawai *et al.* (1979) and in Joseph *et al.* (1981) for hindcasting the waves associated with the above cyclone, an extension of the time interval to cover one more intense wind system in the same month is also made in the present. During the extended period, a much more intense cyclone passed over the the region producing winds with maximum speed of 35 m s^{-1}. We have made use of the wind data prepared by Isozaki and Uji (1973) for the above region and time. A time step of 1 hour and grid spacing of 120 nautical miles are used. The grid system along with the numerical boundaries employed is shown in Fig. 5. The prediction calculations were started 4 days in advance of the first available wave measurement on 16th December, as the results from Joseph *et al.* (1981) had established that 4 days

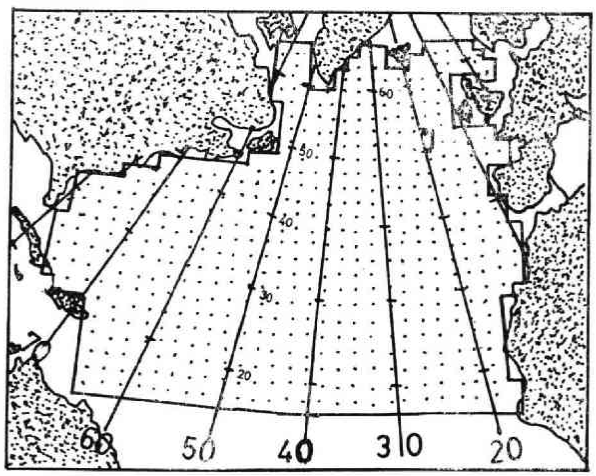

Fig. 5. Grid system used in the North Atlantic with the numerical boundaries. Grid spacing equals to 200 nautical miles. J indicates the weather ship's position during most of the prediction interval.

advance starting of the prediction calculation is sufficient to represent the actual sea condition at the time of the first measurement.

3.1a. Significant waves

A time series of the significant wave heights predicted at J point is shown in Fig. 6 along with the significant wave heights calculated from weather ship's wave

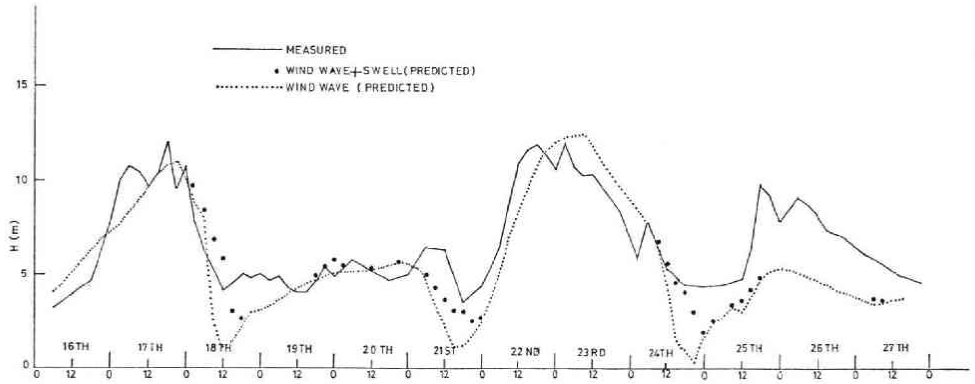

Fig. 6 A comparison of the predicted significant wave heights at the J point with the meaured counterparts.

records (Bretschneider *et al.*, 1962). The predicted significant heights due to the wind waves alone are shown by a dotted line and the circles indicate 'total' significant wave height including the contribution from the nearby passage of swells to J point. The comparison of 'total' significant height with measurements shows generally good agreement. It seems that the extreme wave heights during the two high wave formation intervals (1200 GMT on 17th to 0300 GMT on 18th and 1200 GMT on 22nd to 1200 GMT on 23rd December) are exactly reproduced by the model. Since the reasons behind the minor disagreements in the predictions were well described in Joseph *et al.* (1981), the single dominant disagreement around 0000 GMT on 26th December will be discussed later. The reasons discussed in the above paper included the inaccuracies in the used wind data and the non-coincidence of the J point and the ship positions.

Two examples of spatial distribution of predicted significant wave heights (at 0600 GMT and 1200 GMT on 17th December) corresponding to the first occurrence of high seas around the J point are shown in Fig. 7. The spatial distributions of observed heights for these two times are shown in Fig. 8. The predicted wave pattern in the intense wind region around J point clearly agrees with the observed pattern. In the regions of light winds, ship wave observations are few and contours of height are not drawn.

Regarding the reason behind the dominant underestimation on 26th December, the accuracy of the wind data and the nearness of the ship with the J point were first checked. Each of them is found to be accurate or sufficient as the case may be to

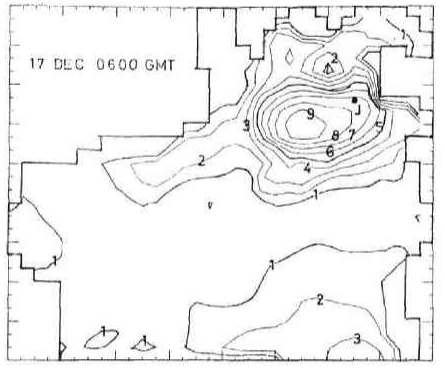

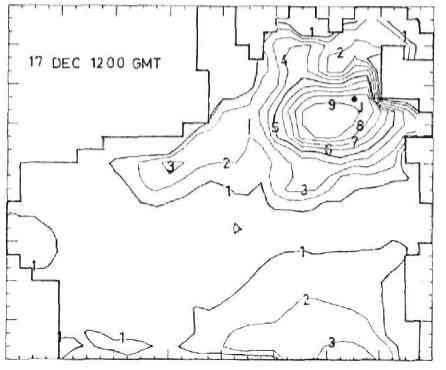

Fig. 7.

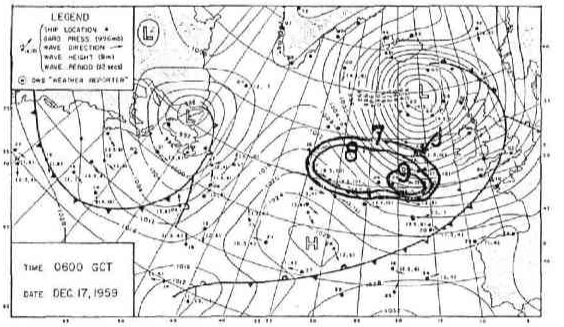

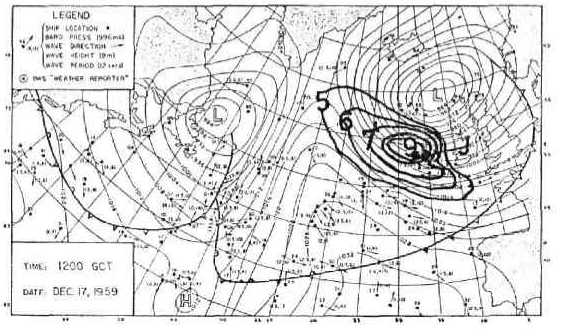

Fig. 8.

Fig. 7. Examples of the predicted spatial significant wave height distribution. The contours are in meters.

Fig. 8. Exmaples of the observed wave and pressure patterns in the North Atlantic on 17th December 1959. Wave height contours (in meters) are drawn on weather charts taken from Wilson (1965).

give a good prediction. But, the wind pattern in the region surrounding the J point showed that a high wind belt existed just south to the J point with winds blowing towards east with a very slight inclination of the order of 10° towards north. In the region northward from J, winds were light with nearly constant direction of northeast. These light winds blowing towards J cannot produce waves up to the observed level by the weather ship. The measured wave spectra (Moskowitz *et al.*, 1963) at the ship point for the above period reveal a wave energy concentration at very low frequencies and this suggests a contribution from swells. These swells might have penetrated to the ship point from the high wave region, but failed to be detected in the present model due to the following reason. As the winds in the high wind belt had nearly constant direction towards east with its northward inclination, in the grid interpolation for the wave energy at a particular grid in this region, no grids north to the selected grid is used. This will give continuous energy growth up to the saturation level. In the low wind belt, the constant northeast direction of the wind also left out the use of any southern grid point in the process of wave energy interpolation. This

means that influences of the high wave belt cannot penetrate to the low wind region of this duration. Once a swell is formed in the high wind region it can easily penetrate into the low wind region. It must happen in actual cases. The formation of swell at the boundary of high wind region is also affected in the model by the method of the selection of wind speed for comparison with the phase speed of the wave packet. In the present situation, it is compared with the high winds present at the grid point since the comparison is done at the grid point in the present model. But in reality of the present situation, the wave packet had experienced low winds during the propagation in the high wind speed gradient region between the wind belt boundaries and had changed to swells. This seems to be the source of the detected high energy swells by the ship. This drawback seems to give higher waves at the boundary of the high wind belt and lower waves in the low wind belt region. This drawback will be again discussed in section 4 with methods for improving the prediction.

3.1b. Wave spectra

Predicted wave spectra for the duration of high seas around the J point (later half of 17th to first half of 18th and from 0000 GMT on 23rd to 0600 GMT on 24th December) are compared with their measured counterpart taken from Bretschneider *et al.* (1962) and Moskowitz *et al.* (1963). The time intervals selected as example correspond to the peak in the wave development and to the next decreasing stages around J point. The comparisons are shown in Fig. 9a, b. Though some differences in the energy level and shifts in the position of the peak frequencies are visible in few cases, the spectra clearly resemble the measured ones. Accuracy in the predicted spectrum is more when the wave field is dominated by wind waves. In general, it can be concluded that the spectral form (6) is sufficient to represent the spectral growth, though it looks much simpler than other spectral forms.

3.2. Hindcasts in intense low systems of Pacific

In this test, an enclosed sea which is free from entrance of swells through numerical boundaries during wave prediction interval is preferred. The Japan Sea seems to satisfy this condition quite well though it is connected to the Pacific Ocean through a few narrow openings mainly at the southern end. As the width of these openings is not much, swell influence through these connections can be neglected. Instead of confining the predictions to the Japan Sea alone, the northwestern Pacific Ocean close to Japan is also included to get a second prediction case of relatively large scale area. A grid spacing of 100 km and time step of 1 hour are used.

For the present, time interval from 1st April to 7th April 1978 was selected. During the above period, the selected region was under intermittent influence of intense low pressure systems as shown in Fig. 10. The pressure patterns at 6 hourly intervals are used in the calculation of gradient wind field in the selected region. The gradient winds are converted to 20 m surface winds by using a constant coefficient of 0.65 and by giving a directional shift of 20°.

Wave prediction calculations were started with the initial condition of zero energy

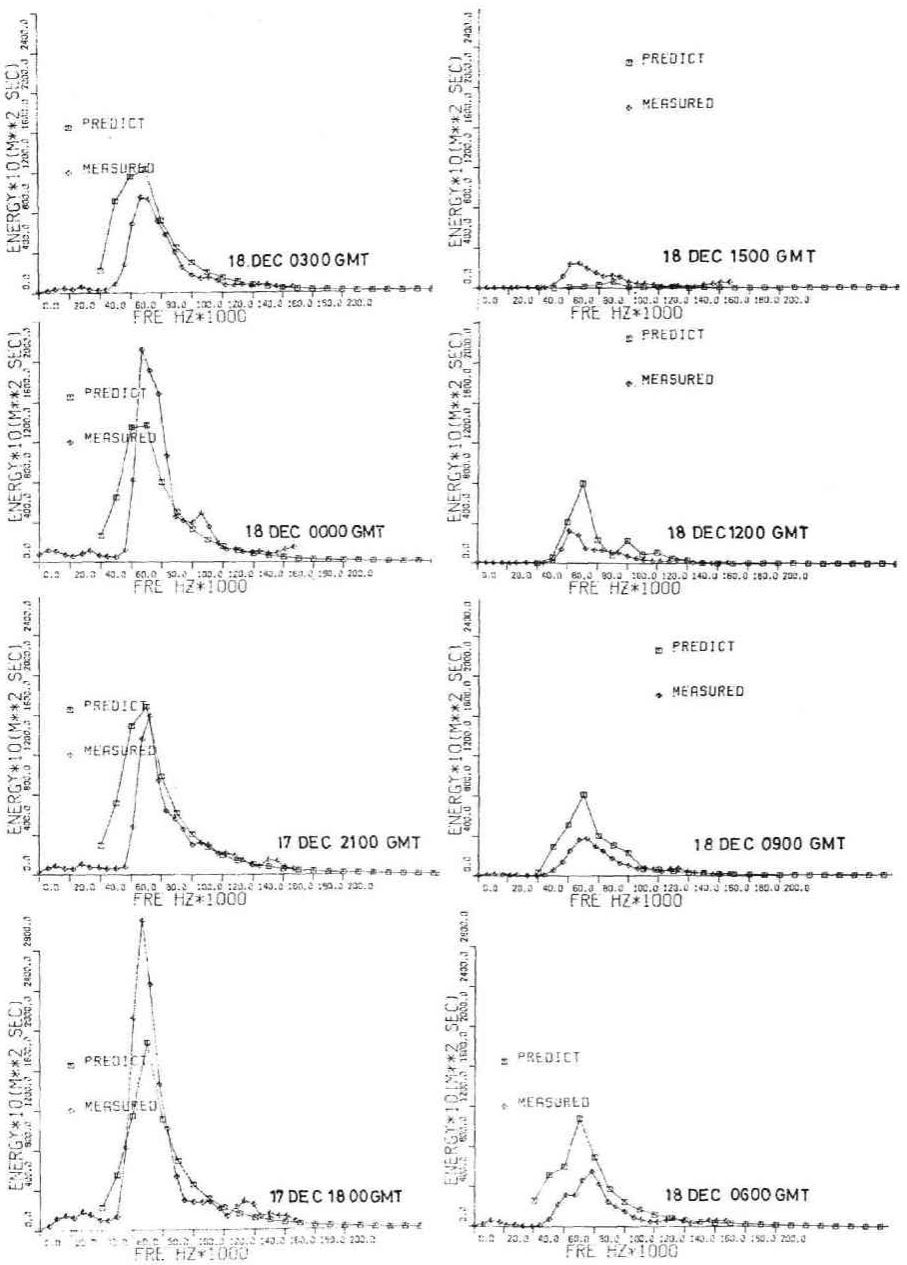

Fig. 9a. Comparisons of predicted wave spectra with the measured counterparts on 17th to 18th December, 1959. One division of the horizontal axis is 0.02 Hz and that of vertical axis 40 m²s.

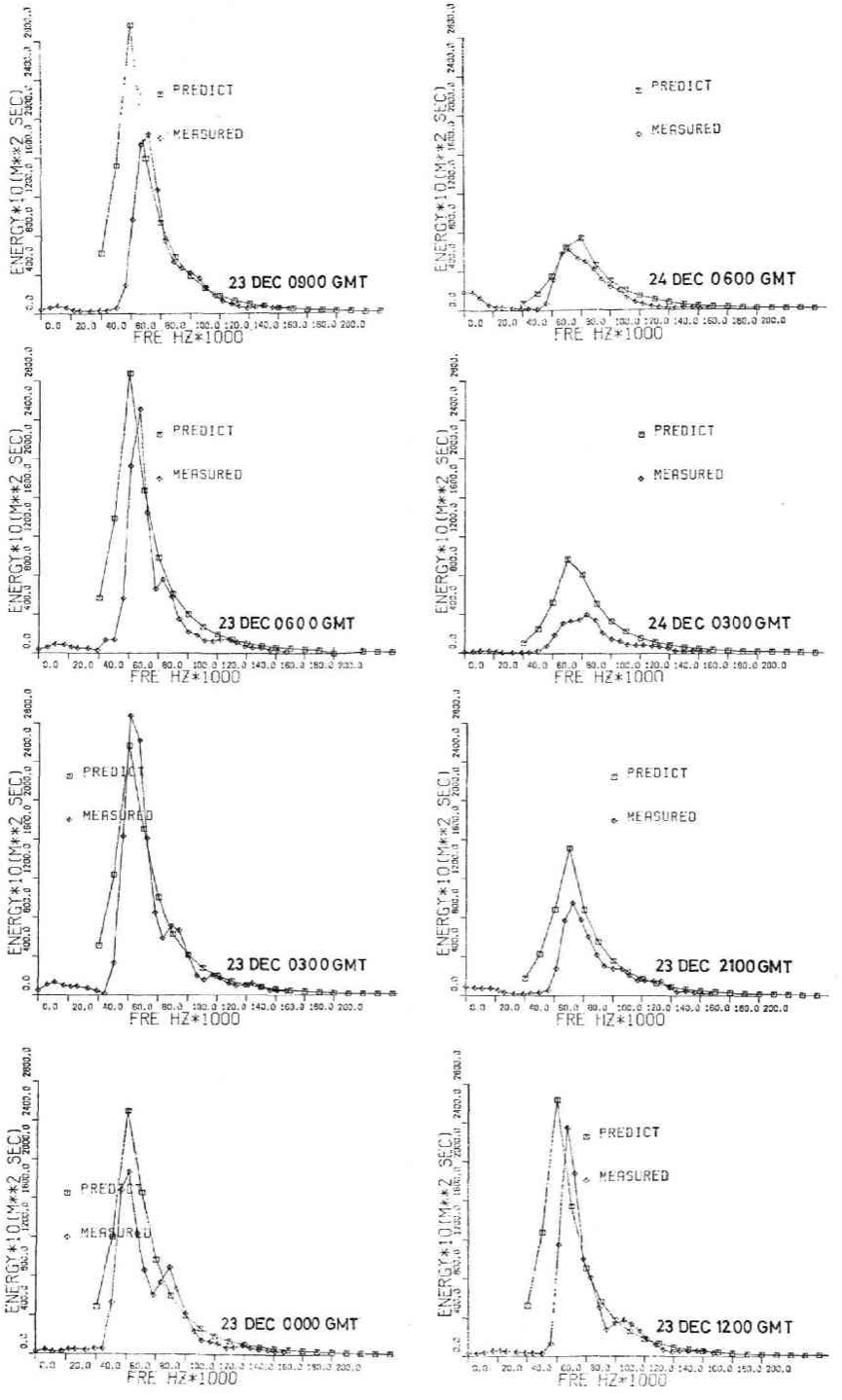

Fig. 9b. Same as in Fig. 9a but on 23rd to 24th December, 1959.

for the entire region. As the wave field needs some initial time for the attainment of actual wave conditions, predictions at the initial durations are not selected for comparison with observations. As the areal extend of this prediction region is nearly half of the Atlantic case, wave patterns after 3 days development are selected for study. A time series comparison at a fixed point as done in the other case is not done due to the lack of a time series observation at an inner grid. Though few coastal grids had such observations, its usage was also left out as the present winds were blowing towards the sea and this gives zero energy to waves at such points due to the present boundary condition. The features of each predicted pattern, shown in Fig. 11 is discussed briefly and compared with their observed counterparts, shown in Fig. 12 which was compiled by Japan Meteorological Agency mainly from visual ship observations of waves.

(i) Wave pattern on 4th

This case represents waves corresponding to maximum winds of 30 m s^{-1} in northern portion of the Pacific. Winds over the Japan Sea were changing from NW to SW direction during the past hours and the Japan Sea had experienced a fetch limited condition. Wind speed over the Japan Sea reached to 16 m s^{-1}, though it was on a decreasing trend at the comparison time. The predicted wave pattern in the Japan Sea has a maximum wave height region on western side of central Japan similar to the observed pattern. Though the region of high waves in prediction and observation is nearly the same, wave heights show a difference of 1 m with the predictions remaining smaller than observations. In Pacific portion also, observed and predicted wave heights show a similar trend of difference.

(ii) Wave pattern on 5th

These waves are associated with low winds of 5 m s^{-1} formed by the movement

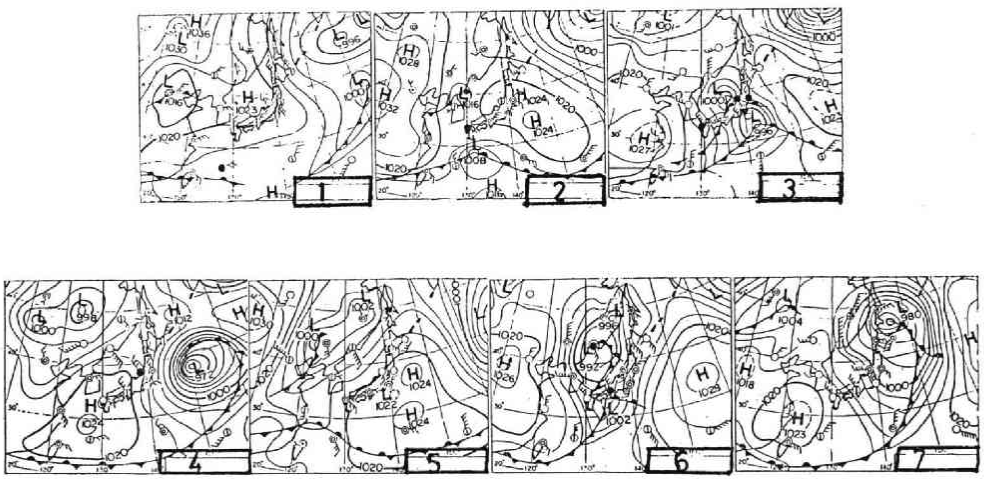

Fig. 10. Pressure patterns over the Japan Sea and the northwestern Pacific Ocean. Number at the corner box of each figure indicates the date in April, 1978. The patterns correspond to 0900 JST.

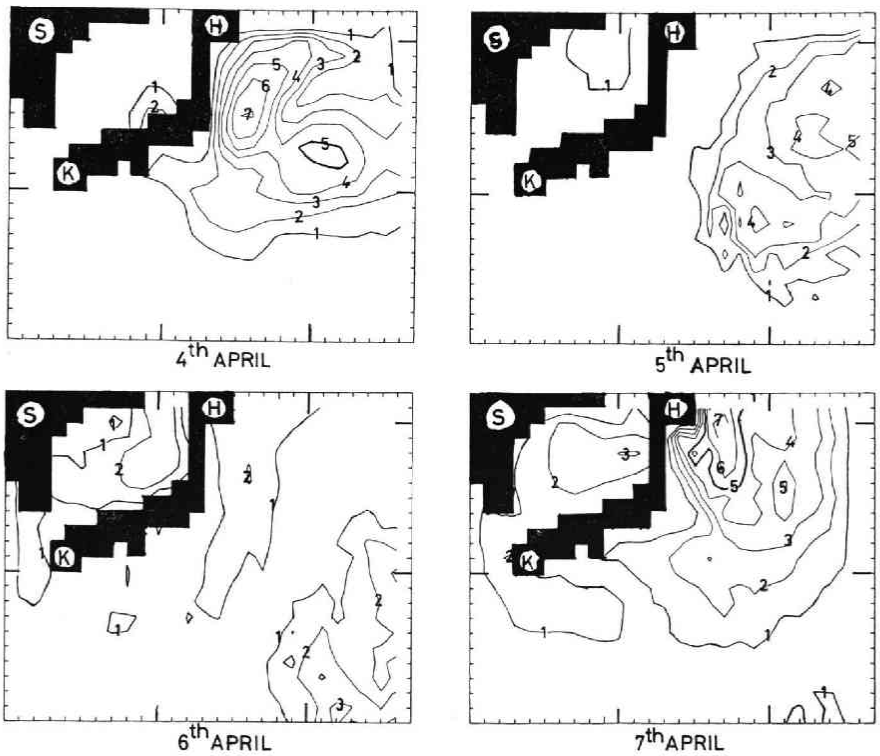

Fig. 11. Examples of predicted spatial distributions of significant wave heights in the Japan Sea and in the northwestern Pacific. Inserted letters mean S for Korea, K for Kyushu and H for Hokkaido. Contours are in meters.

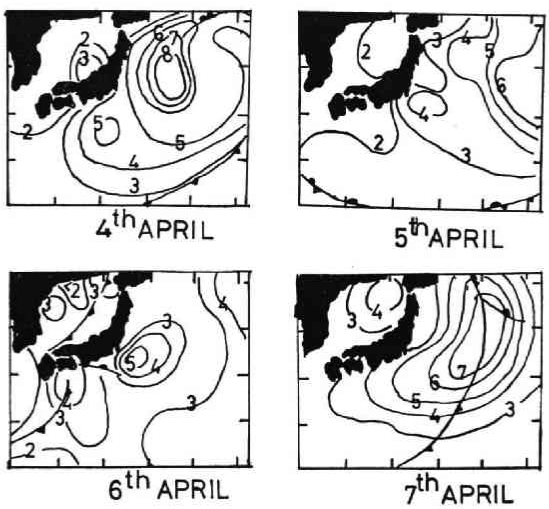

Fig. 12. Examples of observed wave height pattern in the Japan Sea and in the northwestern Pacific, compiled mainly from visual ship wave observations by Japan Meteorological Agency.

of low center out of prediction region. Though relatively strong winds of 15 m s^{-1} were present at northeast corner, the general directions of these intense winds were northwest or northeast. This direction restricts the wave development over northeast corner region as a result of the present boundary condition. Even with this boundary restriction, wave pattern nearly shows the trend, with predictions having an underestimate as mentioned in 4th day example.

(iii) Wave pattern on 6th

In this case, predicted pattern differs much from the observed pattern. Only in the Japan Sea, it shows some resemblance if the underestimation in predictions is not taken into consideration. This case corresponds to time interval after a passage of intense low systems out of the region. The most prominent difference in the predicted pattern is the lack of a high wave region on the eastern side of central Japan. The presence of this region in observations seems to be associated with local high wind fields which may be formed by a rapid development and decay of a localized low pressure system. If total life span of a local pressure system is much shorter than the interval between two pressure field measurements and if such a system occurs in between two pressure field measurements, it may be excluded from wind field calculations and the wind system decided by main pressure patterns may give considerably different winds. A checking of the wind data from ship observations of present case revealed high winds in the region of localized high waves but wind speeds used in the prediction were much lower for these regions. This factor may then explain the difference in the wave patterns.

(iv) Wave pattern on 7th

The high predicted waves close to western coast of northern Japan seem to be formed by intense winds associated with second intense low which remained over Japan sea for a long time. Though position of observed high waves coincides with that of the prediction for the Japan Sea, wave observations show higher values. On the Pacific side, high predicted waves are noticed northeast of Hokkaido. This high region seems to be much deviated from the high wind region and the distribution pattern of waves differs much from the observed pattern. At the location of the observed high wind region, a secondary high predicted wave region is present. A check of wind data of this case showed a manual digitising error during wind field calculation which gave extraordinarily high winds to a region of actually moderate winds. If the most pronounced wave region east of Hokkaido is attributed to this error, the second wave maximum region represents the high wave region formed by the actual intense winds. Though the position of the maximum coincides with that of the intense observed wind and wave region, the predicted heights were 1 to 2 m lesser than the observations.

Taking into consideration all the above mentioned possibility of errors arising in the predictions, it can be stated that the predictions adequately represent the observed wave patterns. In general, there is an underestimate of 2 m or less in wave heights in comparison with ship observations. But, ship's wave data need to be

taken with caution as Verploegh (1961) had shown that the average error in visual observations of wave heights ranges from 0.3 m for 1.5 m high waves to 0.9 m for a 5.5 m wave height. In addition to this, the boundary condition is also seen to influence the predictions. During most of the prediction duration, the observed waves along the southern boundary were 2 to 3 m in heights. This indicates considerable energy entrance through this side. During the times of the intense observed waves, the north and northeast boundaries also seem to influence the predictions owing to the inflowing nature of winds into the region through the boundaries at these durations.

4. Discussion

The results of these examples indicate that the present scheme performs satisfactorily in predicting any desired property of a wave field. But, some predicted spatial patterns indicate non-representation of certain localized features. A few modifications to some of the assumptions employed in the model and slight change in the numerical treatments may improve the predictions. Some possible alterations to the scheme are discussed in the following.

The underestimations in the Pacific case indicate a need for a modification of the boundary condition. Before presenting some possible modifications, we intend to discuss why the influence of boundary is not visible at the intense wave region of the Atlantic case. In the Atlantic case nearly 3 sides were surrounded by coastal boundaries and only the southern side was open. Moreover, the winds were also blowing nearly parallel to the southern boundary during most of the prediction time or outward through this boundary, and for such wind conditions, the boundary effect cannot spread much into the interior region. But, for the Pacific case considerable wave energy was present all along the southern boundary as revealed by the wave observations. During the periods of intense observed waves on 5th, 6th and 7th April, the winds along the north and northeastern boundaries were also blowing into the region, creating boundary problem. The influences from the north and northeastern boundaries seem to dominate the reasons for the underestimates in the high wave region. This implies that some wave energy needs to be given to the boundary grids. If known values are available it is easy, if not, the boundary values at each time step need to be fixed by some assumptions.

In wave predictions (not hindcasts), we have no known value and the boundary values must be assigned by some method. The best way seems to put an energy value for a boundary grid based on some assumptions such as that the gradient of the energy normal to the boundary at the grid point gets vanished. One remaining alternative is the extension of the boundary further, until the boundary influences becomes small at the desired site of wave prediction. But, in this case, with the extension of the prediction duration, the boundary continues its shifting and predictions become impractical after some time, as the computation time gets increased too much and the wind conditions may also become unknown in the wide region. Unless the prediction duration is small, the boundary condition needs to be changed in the first mentioned way.

Next is a problem of the present model, associated with the fine local structures in a wave field. Many fine local observed features are found to be left out in prediction of the Pacific case. This is a problem connected with the fineness in grid spacing. For getting all the fine characters of a wave field, the grids need to be much fine and the time step must be reduced proportionally. Even this much alteration cannot improve the results unless the wind data for the fine meshes are "accurate'. The above term 'accurate" means that the wind field may not be the one decided by the usual method of wind field determination from the pressure fields available at few hour intervals and its further interpolation to still smaller intervals. In such process of wind determination, features in the wind field with time scales less than the interval between the pressure field measurements may get removed. If the pressure measurements are from widely separated spatial points, many local features in the wind field may also be left out. Wave characteristics of time scale less than the time interval between two pressure measurements and space scales less than the distances between two points of pressure measurements may be absent in the results of the present scheme due to the 'inaccuracy' of the wind data. Thus, it seems that the inability of the model to represent few localized wave features is not a direct defect of the scheme. For fine wave characters, fine meshes with fine wind data need to be input, but such fine wind field determination of wide area is a practically difficult task.

The most serious problem found in the course of trials which is directly connected with this prediction scheme, is the inability of the model to represent the wave characteristics close to a 'boundary' separating a strong wind region from a low wind belt which are moving in directions such that the present interpolation of the wind wave energy to the grid point fails to smooth out the gradient in the wind wave energy, as seen in the Atlantic case. As mentioned earlier, the swell formation condition also seems to contribute to the defective predictions for such wind intervals. For avoiding this, first the swell formation chance is to be checked with the wind speed at the new position of each wave packet and then the wind wave part should be interpolated to the grid. The wind speed determination at each new position of the wave packet may increase the computation time considerably. But, critical cases like the exampled ones may occur very rarely in the prediction cases. So, for practical purposes, the original scheme can be applied without the above mentioned change.

Finally, for an estimation of the error in the prediction, the mean value of the difference between the measured and the predicted significant wave heights at a fixed point and its r.m.s. value are calculated. In the present, these calculations are limited to the J point. If all the results at J point are included in the calculation, the mean and r.m.s. show –0.63 m and 1.67 m respectively, for the wave system with the maximum significant height of 15 m. If the defective prediction results associated with the already discussed rare case alone are excluded, the mean and r.m.s. take –0.14 m and 1.36 m, respectively. It need to be mentioned that a further exclusion of inaccurate predictions associated with inaccurate wind data and non-coincidence of J with the ship position, may further improve the r.m.s. and the mean of the differences.

Acknowledgements: The authors wish to express thanks to Dr. I. Isozaki of Meteorological Research Inst., Japan Meteorological Agency and Dr. T. Inoue of Maritime College of Kobe for the supply of a portion of the data used in the work. This study was partially supported by the Grant-in-Aid for Scientific Research by the Ministry of Education, Science and Culture, Project No. 502505, and performed also as a member of the Commission for Development of Ocean-Wave Prediction Techniques, which was organized within the Japan Weather Association in August 1978. The first author expresses his thanks to the Japanese Ministry of Education, Science and Culture for the grant of scholarship during the period of his study and this work forms a part of his doctoral thesis. He also extends his thanks to the National Institute of Oceanography, Goa, India, for granting him study leave.

The computations were performed with FACOM-230-38 and ACOS-NEAC-900 computers of the Tohoku University.

References

Bretschneider, C.L. (1968): Fundamentals of ocean engineering-Part 8. Decay of wind generated waves to ocean swell by significant wave method. *Ocean Industry*, March, 36–39 and 51.

Bretschneider, C.L., H.L. Crutcher, J. Darbyshire, G. Neumann, W.J. Pierson, H. Walden and B.W. Wilson (1962): Data for high wave condition observed by the OWS "Weather Reporter" in December 1959. *Deut. Hydrogr. Zeit.*, **15**, 243–255.

Günther, H., W. Rosenthal, T.J. Weare, B.A. Worthington, K. Hasselmann and J.W. Ewing (1979): A hybrid parametrical wave prediction model. *J. Phys. Oceanogr.*, **84**, 5727–5738.

Hasselmann, K., T.P. Barnett, E. Bouws, H. Carlson, D.E. Cartwright, K. Enke, J.A. Ewing, H. Gienapp, D.E. Hasselmann, P. Kruseman, A. Meerburg, P. Müller, D.J. Olbers, K. Richter, W. Sell and H. Walden (1973): Measurements of wind-wave growth and swell decay during the Joint North Sea Wave Project (JONSWAP). *Deut, Hydrogr. Zeit.*, Suppl. A, **8**, No. 12, 95 p.

Inoue, T. (1967): On the growth of the spectrum of a wind generated sea according to a modified Miles-Phillips' mechanism and its application to wave forecasting. Geophys. Sci. Lab. TR–67–4. New York Univ., 74 p.

Isozaki, I. and T. Uji (1973): Numerical prediction of ocean wind waves. *Pap. Met. Geophys.*, **24**, 207–231.

Joseph, P.S., S. Kawai and Y. Toba (1981): Prediction of ocean waves based on the single-parameter growth equation of wind waves. (II) Introduction of grid method. *J. Oceanogr. Soc. Japan*, **37**, 20–31.

Kawai, S., K. Okada and Y. Toba (1977): Field data support of three-seconds power law and $gu_*\sigma^{-4}$-spectral form for growing wind waves. *J. Oceanogr. Soc. Japan*, **33**, 137–150.

Kawai, S., P.S. Joseph and Y. Toba (1979): Prediction of ocean waves based on the single-parameter growth equation of wind waves. *J. Oceanogr. Soc. Japan*, **35**, 151–167.

Longuet-Higgins, M.S. (1952): On the statistical distribution of the heights of sea waves. *J. Mar. Res.*, **11**, 245–266.

Mitsuyasu, H. (1968): On the growth of the spectrum of wind-generated waves (I). *Rep. Res. Inst. Appl. Mech. Kyushu Univ.*, **16**, 459–482.

Mitsuyasu, H., F. Tasai, T. Suhara, S. Mizuno, M. Ohkusu, T. Honda and K. Rikiishi (1980): Observation of the power spectrum of ocean waves using a cloverleaf buoy. *J. Phys. Oceanogr.*, **10**, 286–296.

Moskowitz, L., W.J. Pierson and E. Mehr (1963): Wave spectra estimated from wave records obtained by the OWS Weather Explorer and the OWS Weather Reporter (II). Technical report prepared for U.S. Navy Oceanographic Office under contract N62306–1042 by New

York University. 23 pp. Geophysical Science Laboratory Report No. 63-5.

Toba, Y. (1972): Local balance in the air-sea boundary processes. I. On the growth process of wind waves. *J. Oceanogr. Soc. Japan*, **28**, 109–121.

Toba, Y. (1973): Local balance in the air-sea boundary processes, III. On the spectrum of wind waves. *J. Oceanogr. Soc. Japan*, **29**, 209–220.

Toba, Y. (1978): Stochastic form of the growth of wind waves in a single-parameter representation with physical implications. *J. Phys. Oceanogr.*, **8**, 494–507.

Tokuda, M. and Y. Toba (1981): Statistical characteristics of individual waves in laboratory wind waves. I. Individual wave spectra and similarity structure. Submitted to *J. Oceanogr. Soc. Japan.*

Verploegh, G. (1961): On the accuracy and the interpretation of wave observations from selected ships. W.M.O. Commission for Maritime Meteorology Working papers.

Wilson, B.W. (1965): Numerical prediction of ocean waves in the North Atlantic for December 1959. *Deut. Hydrogr. Zeit.*, **18**, 114–130.